JVSTA Journal of Vacuum Science & Technology A

X-ray photoelectron spectroscopy, x-ray absorption spectroscopy, and x-ray diffraction characterization of CuO – TiO 2 – CeO 2 catalyst system

M. S. P. Francisco, P. A. P. Nascente, V. R. Mastelaro, and A. O. Florentino

Citation: Journal of Vacuum Science & Technology A **19**, 1150 (2001); doi: 10.1116/1.1345911
View online: http://dx.doi.org/10.1116/1.1345911
View Table of Contents: http://scitation.aip.org/content/avs/journal/jvsta/19/4?ver=pdfcov
Published by the AVS: Science & Technology of Materials, Interfaces, and Processing

X-ray photoelectron spectroscopy, x-ray absorption spectroscopy, and x-ray diffraction characterization of $CuO-TiO_2-CeO_2$ catalyst system

M. S. P. Francisco
Departamento de Física e Ciência dos Materiais, Instituto de Física de São Carlos, Universidade de São Paulo, 13560-970 São Carlos, SP, Brazil

P. A. P. Nascente[a)]
Centro de Caracterização e Desenvolvimento de Materiais, Departamento de Engenharia de Materiais, Universidade Federal de São Carlos, 13565-905 São Carlos, SP, Brazil

V. R. Mastelaro
Departamento de Física e Ciência dos Materiais, Instituto de Física de São Carlos, Universidade de São Paulo, 13560-970 São Carlos, SP, Brazil

A. O. Florentino
Departamento de Química, Instituto de Biociências, Universidade Estadual Paulista, 18618-000 Botucatu, SP, Brazil

(Received 13 September 2000; accepted 11 December 2000)

X-ray photoelectron spectroscopy (XPS), x-ray diffraction (XRD), and x-ray absorption spectroscopy (XAS) techniques have been applied to characterize the surface composition and structure of a series of $CuO-TiO_2-CeO_2$ catalysts. For a small loading of cerium, ceria was mainly dispersed on the titania surface and a minor amount of CeO_2 crystallite appeared. At higher loading of cerium, the CeO_2 phase increased and the atomic Ce/Ti ratio values were smaller than the nominal composition, as a consequence of cerium agglomeration. This result suggests that only a fraction of cerium can be spread on the titania surface. For titanium-based mixed oxide, we observed that cerium is found as Ce^{3+} uniquely on the surface. The atomic Cu/(Ce+Ti) ratio values showed no influence from cerium concentration on the dispersion of copper, although the copper on the surface was shown to be dependent on the cerium species. For samples with a high amount of cerium, XPS analysis indicated the raise of second titanium species due cerium with spin-orbit components at higher binding energies than those presented by Ti^{4+} in a tetragonal structure. The structural results obtained by XAS are consistent with those obtained by XRD and XPS. © *2001 American Vacuum Society.* [DOI: 10.1116/1.1345911]

I. INTRODUCTION

Methanol oxidation to methyl formate is an industrially important reaction because formate is a raw material in the production of formic acid, dimethyl formamide, acetic acid, formamide, and cyanhydric acid. The oxidative catalyze is the most used process, which permits us to obtain a product with higher commercial value from molecules with lower aggregate value.[1,2] Among the active catalytic systems for methanol dehydrogenation, alkaline metal oxide, zinc oxide, and copper-containing catalysts are employed.[1,3,4] Copper-supported catalysts show high catalytic activity and selectivity. A possible explanation for this behavior comes from the fact that metallic oxides, which change the oxidation number from one unit are good oxidation catalysts.[4] Recently, copper supported on titanium oxides has demonstrated a high catalytic performance for steam reforming and dehydrogenation of methanol.[5,6]

According to the literature, there are some disadvantages when TiO_2 is used as support for CuO, such as thermal and mechanical instability, sintering of the support, and active phase and titania phase transformation.[1,7]

The stabilization of the active phase and supported catalysts depends firmly on the characteristics of the support. Cerium oxide is known to improve resistance to thermal loss of the supported catalyst surface area, to stabilize the active phase in a fine dispersed state, and also to improve the catalytic activity.[7] The change in oxidation state is associated with the reversible removal and addition of oxygen because of its low redox potential.[8] This behavior probably explains the improvement described above when cerium is added to the catalytic system. In the alumina modified with ceria Larsson and Andersson[9] evidenced an increase of combustion of CO until CuO particles are formed. They have also studied ethanol oxidation in stationary applications on catalysts consisting of copper oxide supported on titania and ceria-modified titania.[7] Their results showed that ceria enhanced the activity of the copper species and stabilized the surface area of the titania support.

We propose to investigate the catalysts structure after loading cerium and copper oxides to the TiO_2 anatase phase. X-ray diffraction (XRD) was employed to determine the crystalline phases and grain sizes. X-ray absorption spectroscopy (XAS) allowed us to probe the short range order around Ce, Cu, and Ti atoms. X-ray photoelectron spectroscopy

[a)]Author to whom correspondence should be addressed; electronic mail: nascente@power.ufscar.br

(XPS) was used to investigate the chemical changes of the elements present at the surface of the catalysts.

II. EXPERIMENTAL PROCEDURES

Titania-based mixed supports were prepared using the sol–gel technique. Commercial $(NH_4)_2Ce(NO_3)_6$ powder (Vetec) was dissolved in nitric acid aqueous solution (1.5 mol/l). Then, $Cu(NO_3)_2.3H_2O$ powder (Vetec) was added, heated until 353 K and kept at this temperature for 30 min, we denoted the resulted solution A. A second solution B was prepared with tetraisopropyl orthotitanate ($C_{12}H_{28}O_4TiO$, Merck) which was dissolved in isopropyl alcohol (mole rate=1). The solution A was added to solution B and submitted to a 50 W ultrasonic vibration for 2 min. The mixture rested for 24 h in a saturated atmosphere of isopropyl alcohol. Finally, the resulting gel was dried at 383 K for 16 h and than calcined at 723 K for 16 h in air. Solution A was controlled under acid conditions (pH 1–2) in order to guarantee a better salt solubilization and a rapid first step alkoxide group protonation when added to solution B. The amount of water added to solution A was calculated in spite of being suitable for cerium salt solubilization and in excess for alkoxide hydrolysis during its polymerization process. The prepared powder $CuO–CeO_2/TiO_2$ samples are denoted as $Ce_{0.91}O_{1.91}Cu_{0.09}$, $Ti_{0.91}O_{1.91}Cu_{0.09}$, $Ce_{0.09}Ti_{0.82}O_{1.91}Cu_{0.09}$, $Ce_{0.27}Ti_{0.64}O_{1.91}Cu_{0.09}$, and $Ce_{0.41}Ti_{0.41}O_{1.82}Cu_{0.18}$, and express the amount of each component in atomic units.

The x-ray powder diffraction patterns were obtained using an automatic Rigaku Rotaflex diffractometer model RU 200B with Cu $K\alpha$ radiation (40 kV/40 mA, 1.5405 Å) and a nickel monochromator filter. The scanning range was 20°–60° (2θ) with a step size of 0.02° and a step time of 3.0 s. The average crystallite sizes were determined by the Scherrer equation. The broadening of half-height peak widths due to slit sizes and x-ray source characteristics was calculated and was equal to 0.16° (2θ). To determine the instrumental broadening, a reference x-ray pattern from powder Si was recorded. The silicon powder with grain size around 5 μm was used. The identification of crystalline phases was accomplished by comparison with JCPDS file Nos. 21-1272, 43-1002, and 41-254 for titania, ceria, and copper oxide, respectively.

The XAS measurements were carried out at the XAFS beamline of the Brazilian Synchrotron Light Laboratory (LNLS). The experiments were performed in transmission mode. The incident and transmitted photon intensities were determined by means of standard ion chamber detectors. A double crystal Si(111) was used as a monochromator and the energy steps were 0.8 eV for x-ray absorption near-edge spectroscopy (XANES) and 2.0 eV for extended x-ray absorption fine spectroscopy (EXAFS) regions. The measurements were performed by analyzing Ti K edge, Ce L_{III} edge, and Cu K edge at room temperature.

The EXAFS analysis was carried out by a microcomputer using a program set written by Michalowicz,[10] according to the recommended procedures described by the International Workshop on Standards and Criteria in XAFS.[11] After removal and normalization of atomic absorption, the $k^3\chi(k)$ weighted EXAFS oscillation was Fourier transformed to R distance space in the range of 3.2–12 $Å^{-1}$ for Cu and 2.3–9.8 $Å^{-1}$ for Ce. In each case, the Kaiser apodization window with $\tau=2.5$ was used. The energy threshold was selected arbitrarily at the inflexion point of the absorption spectra. The contribution of the first coordination shell was extracted by a back Fourier transform in R space and then fitted using experimental phase and amplitude functions.

A quantitative analysis of the Ce–O shell was made taking a CeO_2 compound as reference ($R_{\mathrm{Ce-O}}=2.34$ Å and $N_{\mathrm{Ce-O}}=8$). To model the Cu–O bond, the phase shift and backscattering amplitude for the Cu–O pair were extracted from a CuO compound setting $N=4$ and $R=1.96$ Å. In all the fittings, the number of free N_{par} parameters was kept smaller than the number of independent N_{ind} points, defined as $N_{\mathrm{ind}}=2\Delta R\Delta k/\pi$, where ΔR is the width of the R-space filter windows and Δk is the actual interval of the fitting in the k space.[11] For the fitting at the Cu and Ce edges, the errors were estimated to be approximately equal to ± 0.01 Å in distance and $\pm 5\%$ in coordination numbers.

The XPS analysis was performed in ultrahigh vacuum (low 10^{-7} Pa range) by using a KRATOS XSAM HS spectrometer, with a Mg $K\alpha$ ($h\nu=1253.6$ eV) x-ray source operated at 15 kV and 15 mA. The powder samples were fixed on a steel holder by a double side adhesive tape, and analyzed as received. An electron flood gun was used to reduce charge effects. The high-resolution spectra were obtained with analyzer pass energy of 20 eV. The binding energies were referenced to an adventitious carbon 1s line set at 284.8 eV. For curve fitting, Gaussian line shapes were used for C 1s, O 1s, and N 1s, and a mixed Gaussian/Lorentzian function for Cu 2p, Ti 2p, and Ce 3d. The Shirley background and a least-square routine were applied. The sensitivity factors for quantitative analysis were referenced to F 1s =1.0.

III. RESULTS AND DISCUSSION

A. X-ray diffraction

XRD patterns of the samples calcined at 723 K are shown in Fig. 1. Despite the larger amount of copper, CuO, and Cu_2O phases were not observed. Following the development of XRD patterns, it is possible to notice a great influence of loading cerium on the $Ti_{0.91}O_{1.91}Cu_{0.09}$ sample in which only a very defined anatase phase could be observed (25.2°/2θ). After ceria addition to the $Ti_{0.91}O_{1.91}Cu_{0.09}$ ($Ce_{0.09}Ti_{0.82}O_{1.91}Cu_{0.09}$ sample), the diffractogram changed, depicting weak broad peaks whose main one was centered at the (101) anatase position, and the major peak of the CeO_2–cerianite phase was barely visible (28.2°–28.3°/2θ). After addition of 27% and 45% of cerium ($Ce_{0.27}Ti_{0.64}O_{1.91}Cu_{0.09}$ and $Ce_{0.45}Ti_{0.46}O_{1.91}Cu_{0.09}$ samples), the peaks related to the CeO_2 phase become more pronounced and easily indexed, and only the main peak related to the TiO_2 phase could be observed ($\sim$25.2°/2θ).

The observation that bulk CuO is segregated at higher copper contents in Cu–Ce(La)–O catalysts was done by Liu

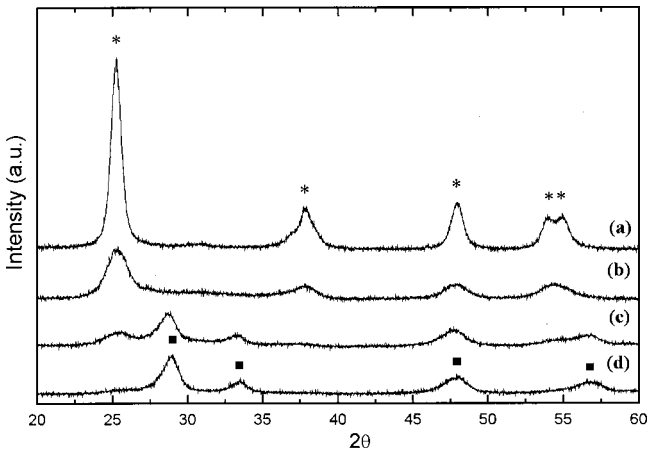

FIG. 1. XRD patterns: (a) $Ti_{0.91}O_{1.91}Cu_{0.09}$, (b) $Ce_{0.09}Ti_{0.82}O_{1.91}Cu_{0.09}$, (c) $Ce_{0.27}Ti_{0.64}O_{1.91}Cu_{0.09}$, (d) $Ce_{0.41}Ti_{0.41}O_{1.82}Cu_{0.18}$, calcined at 723 K. TiO_2–anatase phase (*) and CeO_2–ceranite phase (■).

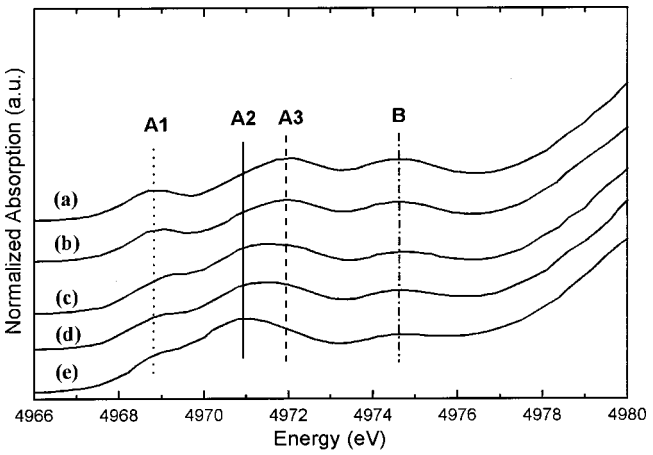

FIG. 2. Ti *K*-edge XANES spectra of: (a) TiO_2–anatase phase, (b) $Ti_{0.91}O_{1.91}Cu_{0.09}$, (c) $Ce_{0.09}Ti_{0.82}O_{1.91}Cu_{0.09}$, (d) $Ce_{0.27}Ti_{0.64}O_{1.91}Cu_{0.09}$, and (e) $Ce_{0.41}Ti_{0.41}O_{1.82}Cu_{0.18}$.

and Flytzani-Stephanopoulos.[12] They concluded that only a small amount of copper is necessary to promote the CO oxidation. The excess of copper forms bulk CuO particles, which contributes little to the catalyst activity. Copper-containing phases were not detected in Cu/TiO_2 catalysts with lower copper loading as a consequence of the sensitivity and size limits of the XRD technique.[13] Larsson and Andersson[7,9] have studied $CuO_x-CeO_2-Al_2O_3$ and $CuO_x-CeO_2-TiO_2$ catalyst systems. For low copper loading, in the first system they identified Cu atoms as a copper aluminate surface phase, and in the second system they detected no peak from the CuO phase. They observed the presence of bulk CuO crystallites in both systems only for high loading. They concluded that the distribution of copper species depends not only on the copper oxide loading but also on the ceria loading.

Our XRD results revealed the presence of only two crystallographic phases: TiO_2 anatase and CeO_2 cerianite. The amount of both phases depends on the support composition, but it is independent of the copper content. The absence of Cu phases in our samples is in agreement with the results recently published.[7,9] As the amount of copper increased, we can state that copper atoms are well dispersed on the support structure.

The titania grain size was calculated by the Scherrer equation for each sample. We observed a trend toward smaller TiO_2 crystallites as cerium was added: the titania grain size presented by $Ti_{0.91}O_{1.91}Cu_{0.09}$ was equal to 12.3 nm and by the sample with the highest amount of cerium ($Ce_{0.45}Ti_{0.46}O_{1.91}Cu_{0.09}$ sample) 2.4 nm. Furthermore, due to the fact that any significant peak shift of the crystalline phases mentioned above was observed, the formation of a solid solution can be discarded.

B. XAS measurements

1. Ti K-edge: XANES spectra

The Ti *K*-edge spectrum for titania at the anatase phase obtained as a reference is very similar to that presented in the literature.[14,15] All catalysts seemed to have titanium at the anatase phase, as it was identified by XRD. Figure 2 shows the pre-edge region of the Ti absorption edge. For all samples at least three pre-edge peaks were presented and some of them had their intensities strongly modulated as cerium concentration is increased: the intensities of $A3(4971.9\,\text{eV})$ and $A1(4968.8\,\text{eV})$ peaks decreased and the $A2$ peak (4970.9 eV) became clear, appearing to dominate in the $Ce_{0.41}Ti_{0.41}O_{1.82}Cu_{0.18}$ sample. The intensity of the *B* peak (4974.6 eV) did not change significantly.

In a previous study of the Ti *K* pre-edge, Chen *et al.*[14,15] investigated titanium dioxide nanoparticles (19 Å) which had their Ti *K*-edge spectra compared to the spectrum of octahedral Ti sites in bulk anatase (500 Å). The XANES data revealed the rise of titanium in the surface in penta-coordinated sites as a result of distortions of Ti sites in smaller TiO_2 nanoparticles. Chen *et al.*[14] distinguished the coexistence of the surface layer from bulk TiO_2 by measuring XAS spectra of particles with many different sizes and observing the changes in the spectral features. As the particle size became smaller, more Ti atoms were on the surface in an anisotropic environment, which caused distortions around Ti atoms from an octahedral TiO_6 unit.[14] Farges *et al.*[16] associated titanium with $^{[4]}$Ti, $^{[5]}$Ti, and $^{[6]}$Ti coordination to the following peak positions: 4969.5, 4970.5, and 4971.5 eV.

Our results indicated that due to the addition of cerium to the support, the number of Ti atoms in an octahedral TiO_2 structure decreased as a consequence of the decrease of titanium particle size. Moreover, the intensity of the $A3$ peak, which is assigned to $^{[6]}$Ti coordination decreased, reinforcing the previous statement.

2. Ce L_{III}-edge results: XANES/EXAFS spectra

Figure 3 shows the Ce L_{III} XANES spectra of the catalyst samples together with CeO_2 reference spectrum in which the cerium atom is tetravalent, surrounded by oxygen ions filling the tetrahedral interstitial sites. The two major peaks (denoted *a* and *b*) of CeO_2 spectrum are in agreement with the

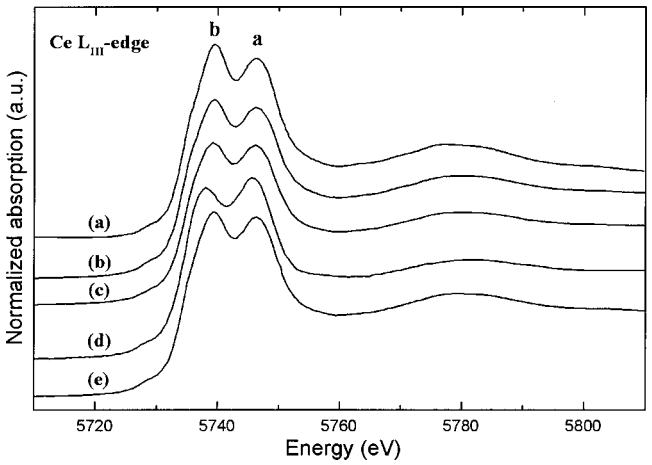

FIG. 3. Ce L_{III}-edge XANES spectra of: (a) CeO_2 reference, (b) $Ce_{0.91}O_{1.91}Cu_{0.09}$, (c) $Ce_{0.27}Ti_{0.64}O_{1.91}Cu_{0.09}$, (d) $Ce_{0.09}Ti_{0.82}O_{1.91}Cu_{0.09}$, and (e) $Ce_{0.41}Ti_{0.41}O_{1.82}Cu_{0.18}$.

literature results.[17] These two components were also detected in the catalyst samples with an intensity ratio and energy position close to that found in the CeO_2 sample.

Figure 4 presents a comparison of EXAFS spectra for CeO_2 and the catalysts. The EXAFS spectra of the $Ce_{0.27}Ti_{0.64}O_{1.91}Cu_{0.09}$ and $Ce_{0.41}Ti_{0.41}O_{1.82}Cu_{0.18}$ catalysts are comparable to the CeO_2 spectrum, whereas the spectrum of the $Ce_{0.09}Ti_{0.82}O_{1.91}Cu_{0.09}$ sample is rather different. This difference can also be observed in the Fourier transform spectra displayed in Fig. 4. For the samples with a higher amount of cerium, the second peak (between 3 and 5 Å) was observed, although its intensity was lower than in the CeO_2. This peak is related to Ce–Ce and Ce–O bonds (second neighbors).

The phase and amplitude used to simulate the EXAFS spectra were obtained from the CeO_2 reference and the results are presented in Table I. Both $Ce_{0.27}Ti_{0.64}O_{1.91}Cu_{0.09}$ and $Ce_{0.41}Ti_{0.41}O_{1.82}Cu_{0.18}$ samples showed a first coordination shell similar to that of CeO_2. A better simulation was obtained for the $Ce_{0.09}Ti_{0.82}O_{1.91}Cu_{0.09}$ sample when two distances for the first coordination shell were considered, although the average number of first neighbors was equal to 8 and the average Ce–O distance was 2.32 Å.

3. Cu *K-edge results: XANES/EXAFS spectra*

The Cu *K*-edge XANES spectra were collected for two copper patterns, CuO (Cu^{2+} in a square planar symmetry) and Cu_2O (Cu^{1+} coordinated by two oxygen atoms), and for the catalysts. The XANES spectra are shown in Fig. 5. The CuO and Cu_2O XANES spectra presented edge energies at 8984.3 and 8980.5 eV, respectively, whereas the catalysts presented a transition positioned at approximately 8986.4 eV. These transitions were ascribed to a dipole-enabled electronic transition of $1s \rightarrow 4p$.[18] Moreover, the *A* peak (9016.0 eV) disappeared and the *B* peak (8997.9 eV) broadened when cerium was added to the support. Thus, the catalysts presented quite different XANES spectra when compared to the CuO and Cu_2O reference compounds.

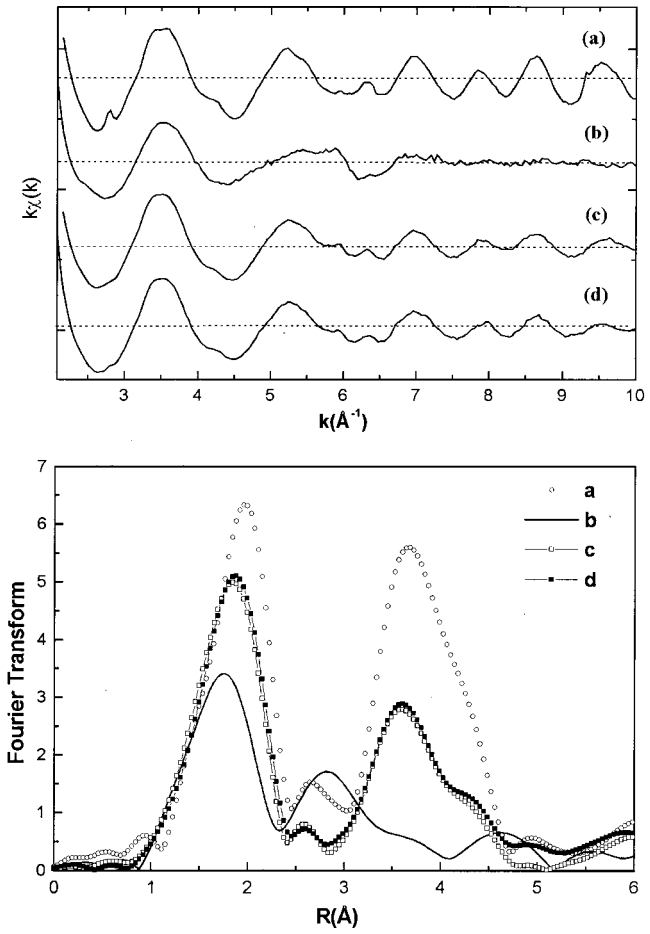

FIG. 4. (Top) Ce L_{III}-edge EXAFS spectra of: (a) CeO_2 phase, (b) $Ce_{0.09}Ti_{0.82}O_{1.91}Cu_{0.09}$, (c) $Ce_{0.27}Ti_{0.64}O_{1.91}Cu_{0.09}$, and (d) $Ce_{0.41}Ti_{0.41}O_{1.82}Cu_{0.18}$. (Bottom) Fourier transform of the Ce L_{III}-edge EXAFS spectra of: (a) CeO_2 phase, (b) $Ce_{0.09}Ti_{0.82}O_{1.91}Cu_{0.09}$, (c) $Ce_{0.27}Ti_{0.64}O_{1.91}Cu_{0.09}$, and (d) $Ce_{0.41}Ti_{0.41}O_{1.82}Cu_{0.18}$.

The Cu-*K* edge EXAFS spectra presented in Fig. 6 look very similar, but they differ from the CuO EXAFS spectrum. The Fourier transform EXAFS spectra are presented in Fig. 6. The position of the main peak, which corresponds to the first Cu–O coordination shell, is similar to that of all the catalysts and CuO. Backscattering phase and amplitude were extracted from the CuO compound to provide quantitative structural information of the first Cu–O coordination shell. The simulation results are presented in Table I, showing a coordination number approximately equal to 4.0 for all samples and a Cu–O mean bond length at around 1.95 Å. A decrease in the intensity of the first peak was observed in the Fourier transform spectra of the catalyst samples when compared to the CuO sample as a result of the Debye–Waller factor increasing.

Regarding more distant shells, it can be observed that the Fourier transform spectra of all catalyst samples show a second peak located between 2.2 and 3 Å, which is related mainly to the Cu–Cu first neighbors. This peak in the catalysts is less intense than that of the CuO compound. This difference is probably due to the presence of Ti and Ce atoms in the structure of the catalyst samples.

TABLE I. Simulation results for Ce L_{III}-edge and Cu K-edge EXAFS spectra.

Sample	Ce L_{III} edge			Cu K edge		
	N/Ce–O (±0.5)	R (Å) (±0.02)	σ (Å) (±0.01)	N/Cu–O (±0.4)	R (Å) (±0.01)	σ (Å) (±0.01)
CuO	—	—	—	4.0	1.96	—
$Ti_{0.91}O_{1.91}Cu_{0.09}$	—	—	—	4.2	1.95	0.04
CeO_2	8.0	2.34	—	—	—	—
$Ce_{0.09}Ti_{0.82}O_{1.91}Cu_{0.09}$	6.2	2.25	0.07	3.8	1.95	0.05
	2.2	2.40	0.13	···	···	···
$Ce_{0.27}Ti_{0.64}O_{1.91}Cu_{0.09}$	7.9	2.32	0.06	—	—	—
$Ce_{0.41}Ti_{0.41}O_{1.91}Cu_{0.18}$	7.8	2.31	0.06	4.1	1.96	0.06

C. XPS analysis

Information about changes in the oxidation number and structure from copper, cerium, and titanium due to loading cerium were obtained by XPS analysis. Binding energy values of the main peaks in the XPS of references and samples are summarized in Table II.

Figure 7 shows the Ti $2p$ XPS spectra of samples and TiO_2–anatase. Lu *et al.*[19] reported the Ti $2p_{3/2}$ peaks at 458.8, 457.5, and 455.1 eV for TiO_2, Ti_2O_3, and TiO, respectively. The Ti $2p$ doublet of TiO_2–anatase presented its spin-orbit components at 459.0 eV($2p_{3/2}$) and 464.6 eV($2p_{1/2}$) with full width at half maximum and relative intensity (2:1) in good agreement with results from the literature.[19] We deconvoluted the $2p_{3/2}$ and $2p_{1/2}$ peaks of the $Ti_{0.91}O_{1.91}Cu_{0.09}$ sample by single components each, corresponding to Ti^{4+} in a tetragonal structure. Otherwise, we fitted the $2p$ spectrum of the $Ce_{0.09}Ti_{0.82}O_{1.91}Cu_{0.09}$ sample by two curves at each peak. We assigned the Ti $2p_{3/2}$ peak at lower binding energy (459.2 eV) to titanium in a tetragonal structure and the Ti $2p_{3/2}$ peak at higher binding energy (460.8 eV) to species at the same oxidation number 4+. Analyzing the intensities from $2p_{3/2}$ peaks of the two titanium species in the $Ce_{0.09}Ti_{0.82}O_{1.91}Cu_{0.09}$ sample, the tetragonal structure is predominant on the surface. The spin-orbit components in the spectra of $Ce_{0.27}Ti_{0.64}O_{1.91}Cu_{0.09}$ and $Ce_{0.27}Ti_{0.64}O_{1.91}Cu_{0.09}$ samples were also better fitted taking into account the presence of two species. The number of distorted species from tetragonal structure on the surface became higher with cerium addition.

Similar results to ours were obtained for IrO_2–TiO_2–CeO_2 electrocatalysts.[20] The Ti $2p$ spectra became larger with shifts to higher energy values for cerium-

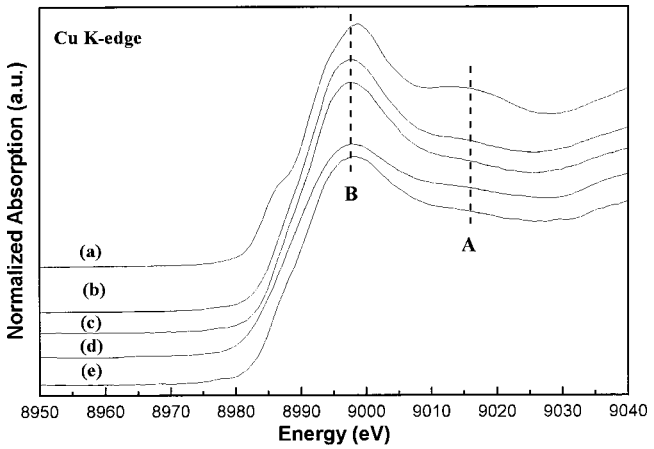

FIG. 5. Cu K-edge XANES spectra of: (a) Cu_2O, (b) CuO, (c) $Ti_{0.91}O_{1.91}Cu_{0.09}$, (d) $Ce_{0.09}Ti_{0.82}O_{1.91}Cu_{0.09}$, (e) $Ce_{0.27}Ti_{0.64}O_{1.91}Cu_{0.09}$, and (f) $Ce_{0.41}Ti_{0.41}O_{1.82}Cu_{0.18}$.

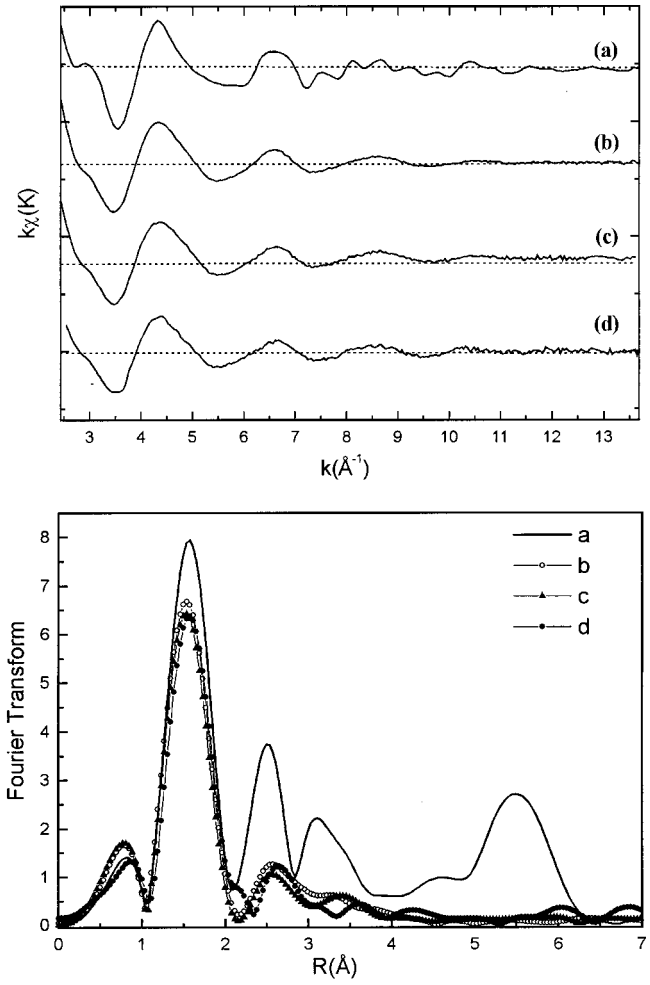

FIG. 6. (Top) Cu K-edge EXAFS spectra: (a) CuO, (b) $Ti_{0.91}O_{1.91}Cu_{0.09}$, (c) $Ce_{0.09}Ti_{0.82}O_{1.91}Cu_{0.09}$, and (d) $Ce_{0.41}Ti_{0.41}O_{1.82}Cu_{0.18}$; (Bottom) Fourier transform of Cu K-edge EXAFS spectra of: (a) CuO, (b) $Ti_{0.91}O_{1.91}Cu_{0.09}$, (c) $Ce_{0.09}Ti_{0.82}O_{1.91}Cu_{0.09}$, and (d) $Ce_{0.41}Ti_{0.41}O_{1.82}Cu_{0.18}$.

TABLE II. XPS binding energy values; XPS atomic ratios as a function of Ce content for the references and samples; u'''/I_{Total} and $(u'+v')/I_{\text{Total}}$ ratios were calculated from Ce $3d$ peaks of reference and samples.

	B.E. eV				
				O $1s$	
Sample	Cu $2p_{3/2}$	Ti $2p_{3/2}$	Ce $3d_{5/2}$	OH^-	O_{lattice}
CeO_2	—	—	882.7	531.7	529.4
TiO_2	—	459.0	—	531.7	530.1
$Ce_{0.91}O_{1.91}Cu_{0.09}$	933.7	—	882.3	531.4	529.4
$Ti_{0.91}O_{1.91}Cu_{0.09}$	933.7	459.0	—	531.4	529.4
$Ce_{0.09}Ti_{0.82}O_{1.91}Cu_{0.09}$	933.6	459.2/460.8	883.2	532.1	530.5
$Ce_{0.27}Ti_{0.64}O_{1.91}Cu_{0.09}$	933.7	429.3/460.6	882.6	531.5	530.0
$Ce_{0.45}Ti_{0.46}O_{1.91}Cu_{0.09}$	933.8	458.7/460.5	882.2	531.6	529.9
CuO	933.9	—	—	531.8	529.9
Cu_2O	932.1	—	—	531.9	530.2

	Atomic ratio					
	Ce/Ti	Cu/(Ti+Ce)	Cu/Ce	Cu/Ti	u'''/I_{Total}	$(u'+v')/I_{\text{Total}}$
CeO_2					0.11	0.14
$Ce_{0.91}O_{1.91}Cu_{0.09}$	—	0.17	0.17	—	···	···
$Ti_{0.91}O_{1.91}Cu_{0.09}$	—	0.14	—	0.14	···	···
$Ce_{0.09}Ti_{0.82}O_{1.91}Cu_{0.09}$	0.10	0.17	1.91	0.19	0.07	0.27
$Ce_{0.27}Ti_{0.64}O_{1.91}Cu_{0.09}$	0.33	0.15	0.60	0.20	0.08	0.20
$Ce_{0.45}Ti_{0.46}O_{1.91}Cu_{0.09}$	0.64	0.15	0.41	0.26	0.09	0.22

rich samples, suggesting that this element is present in more than one species. Strong interaction between TiO_2 and SiO_2 in mixed oxides was reported to present higher Ti $2p_{3/2}$ binding energy than the value for pure TiO_2.[21] This upward shift was explained by the increase in the interatomic potentials due to the decrease of the coordination number of Ti and the shortening of the Ti–O bond. The XPS result indicating that the presence of Ti^{4+} in the tetragonal structure decreased with cerium addition on the surface titanium is corroborated with our Ti K-edge XANES and grain size analyses.

Figure 7 shows the Ce $3d$XP spectra, where six peaks corresponding to three pairs of spin-orbit doublets were identified and ascribed to Ce (IV) and the other two peaks were ascribed to Ce (III). The spin-orbit doublets are commonly denoted u and v and represent the $3d_{5/2}$ and $3d_{3/2}$ states, respectively, in the range 880–920 eV.[22] The v and v'' peaks have been attributed to a mix of $3d^9 4f^2(\text{O}\,2p^4)$ and $3d^9 4f^1(\text{O}\,2p^5)\text{Ce}(IV)$ final states, and v''' peak to $3d^9 4f^0(\text{O}\,2p^6)\text{Ce}(IV)$ final state.[7] The v' peak corresponds to the $3d^9 4f^1(\text{O}\,2p^6)\text{Ce}(III)$ final state.[7] The series of u structures from the $3d_{3/2}$ level can be explained in the same way. The ratio between the u''' intensity and the total intensity of Ce $3d$ lines depends on the Ce^{4+}/Ce^{3+} ratio. Together with u''' peak behavior, Ce^{4+} reduction causes the v' and u' increase.[7,22] Those ratios calculated for reference and samples are displayed in Table II, where the trends toward smaller u'''/I_{Total} ratio and higher $(u'+v')/I_{\text{Total}}$ ratio with cerium addition may be observed. Then, samples containing cerium seem to have part of this element as Ce^{3+}. Although the possibility of Ce^{3+} presence in the catalysts cannot be ruled out by XAS analysis, the existence of Ce^{3+} must be limited only to the surface.

The Cu $2p$XPS results are presented in Table II. The Cu $2p$XP spectrum of CuO was easily identified by the satellite at about 940–945 eV and the $2p_{3/2}$ main peak at 934.2 eV.[1] The Cu $2p$XP spectra for both $Ti_{0.91}O_{1.91}Cu_{0.09}$ and $Ce_{0.91}O_{1.91}Cu_{0.09}$ references were fitted by only one peak centered at 933.7 eV. The satellite for the former one (~944.4 eV) appeared more prominent than for the last one. For the catalyst spectra, the Cu $2p_{3/2}$ components were positioned very close to each other at 933.8 eV. The catalysts presented a weak satellite, probably due to their low copper concentration. All catalysts had their copper species as dispersed Cu^{2+} since no copper peak was identified by XRD.

XP spectra were also obtained in order to analyze the surface composition changes caused by loading cerium to the support. The surface ratios and nominal composition as a function of Ce content of samples are presented in Table II. The atomic Ce/Ti ratio values increased with cerium content on the support. The $Ce_{0.09}Ti_{0.82}O_{1.91}Cu_{0.09}$, $Ce_{0.27}Ti_{0.64}O_{1.91}Cu_{0.09}$, and $Ce_{0.45}Ti_{0.46}O_{1.91}Cu_{0.09}$ samples presented their respective atomic Ce/Ti ratios as 9%, 21%, and 36% lower than their nominal compositions. It seems that for low cerium concentration most of this element is simply dispersed on the matrix. As cerium concentration increases, the dispersed species originated the second cerium species. The XRD data indicated an evolution of the CeO_2 phase: the $Ce_{0.09}Ti_{0.82}O_{1.91}Cu_{0.09}$ sample presented only the major diffraction peak related to this phase, while the $Ce_{0.27}Ti_{0.64}O_{1.91}Cu_{0.09}$ and $Ce_{0.45}Ti_{0.46}O_{1.91}Cu_{0.09}$ samples showed a very defined ceria diffraction pattern. Moreover, XAS data showed that cerium in the $Ce_{0.09}Ti_{0.82}O_{1.91}Cu_{0.09}$ sample had its Ce–O distance distorted from the CeO_2 reference and from other samples with higher cerium concentration. So, our results revealed that a small amount of ceria

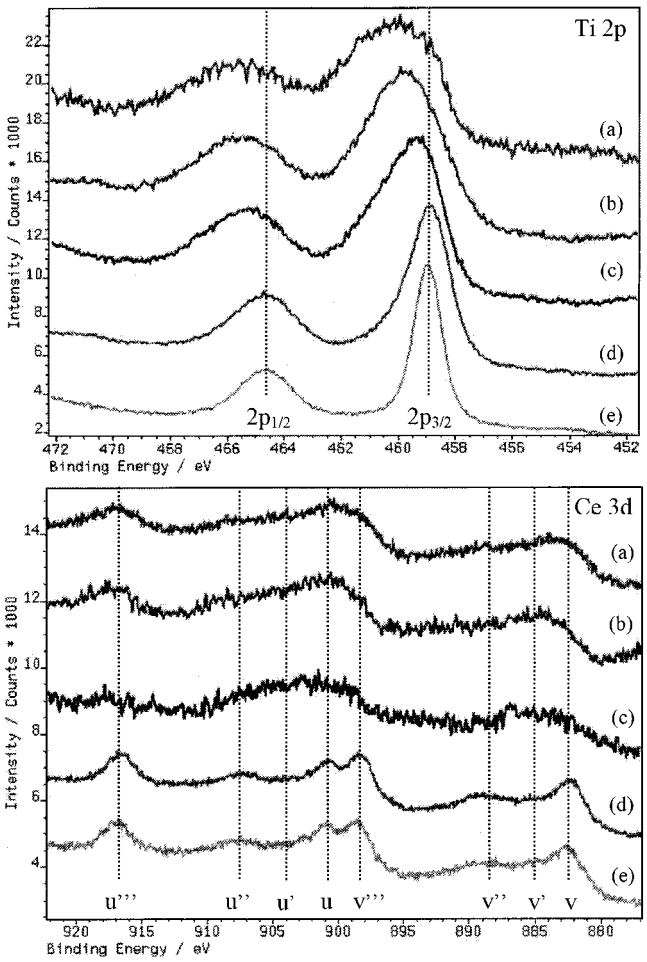

FIG. 7. (Top) Ti $2p$ XP spectra of: (a) $Ce_{0.45}Ti_{0.46}O_{1.91}Cu_{0.09}$, (b) $Ce_{0.27}Ti_{0.64}O_{1.91}Cu_{0.09}$, (c) $Ce_{0.09}Ti_{0.82}O_{1.91}Cu_{0.09}$, (d) $Ti_{0.91}O_{1.91}Cu_{0.09}$, and (e) TiO_2. (Bottom) Ce $3d$ XP spectra of: (a) $Ce_{0.45}Ti_{0.46}O_{1.91}Cu_{0.09}$, (b) $Ce_{0.27}Ti_{0.64}O_{1.91}Cu_{0.09}$, (c) $Ce_{0.09}Ti_{0.82}O_{1.91}Cu_{0.09}$, (d) $Ce_{0.91}O_{1.91}Cu_{0.09}$, and (e) CeO_2.

could be presented in a dispersed form on the support (invisible by XRD). An excess of CeO_2 caused its crystallization. Other investigators[7] have reported that a limited amount of cerium can be confined to the titania in order to stabilize it, and the excess is segregated on the CeO_2 phase.

Comparing the atomic Cu/Ce ratio of the $Ce_{0.91}O_{1.91}Cu_{0.09}$ sample with the Ti/Ce atomic ratio of the $Ti_{0.91}O_{1.91}Cu_{0.09}$ sample, the former was 41% higher than its nominal composition, while the later was only 29%. Thus, copper is more exposed in pure ceria than in titania matrix. From the atomic Cu/(Ti+Ce) ratio value of the samples with cerium, we calculated an average raise from the nominal composition equal to 41%. This result suggests that copper dispersion on the mixed support is independent from cerium concentration.

The atomic Cu/Ce ratio values from all ceria-modified titania samples presented the same raise from nominal composition (an average value equal to 48%), while the Cu/Ti values suffered influence from cerium addition. These ratios decreased with cerium loading compared to their respective nominal composition. A Ti-surface enrichment probably occurred due to titania size decrease as the results from XAS and XRD indicated, in agreement with the titanium second species observed by XPS analysis. The copper dispersion must be more connected to ceria since we observed a cerium segregation with cerium addition, and a higher copper content on the ceria surface than on the titania support.

IV. CONCLUSIONS

The amount of observed phases depends on the support composition, but it is independent of copper content. XPS and XAS analyses suggest that CuO is in the form of small crystallized grains well dispersed on the surface of the mixed support structure, as we observed no CuO bulk phases, even for high copper content. According to this statement, all the samples presented a distorted local order of copper shell due to the presence of Ti and Ce. XPS surface analysis indicated that copper dispersion on the mixed support suffered no influence of cerium concentration, but it is dependent on the cerium species.

The trend toward smaller TiO_2 crystallites with cerium addition was evidenced by XRD measurements, surface area decrease, changes in Ti K post-edge region in the XANES spectra, and the appearance of a second species with higher Ti $2p_{3/2}$ binding energy in the XP spectra. This trend is related to a decrease of the Ti coordination number.

A higher cerium local distortion was observed in XAS analysis for low cerium concentration, implying that CeO_2 is mainly in a dispersed form on the titanium surface. This analysis did not evidence cerium distortion for samples containing a higher amount of CeO_2.

ACKNOWLEDGMENTS

This work has been supported from FAPESP and CNPq Brazilian agencies. This research was partially performed at LNLS, Brazil.

[1]A. Guerrero-Ruiz, I. Rodriguez-Ramos, and J. L. G. Fierro, Appl. Catal. **72**, 119 (1991).
[2]J. M. Tatibouët, Appl. Catal., A **148**, 213 (1997).
[3]L. Domokos, T. Katonaand, and Á. Molnàr, Catal. Lett. **40**, 215 (1996).
[4]G. C. Bond, *Catalysis by Metal*, 1st ed. (Academic, London, 1962).
[5]N. Takezawa and N. Iwasa, Catal. Today **36**, 45 (1997).
[6]J. P. Breen and J. R. H. Ross, Catal. Today **51**, 521 (1999).
[7]P.-O. Larsson and A. Andersson, J. Catal. **179**, 72 (1998).
[8]H. Inaba and H. Tagawa, Solid State Ionics **83**, 1 (1996).
[9]P.-O. Larsson and A. Andersson, Appl. Catal. B **24**, 175 (2000).
[10]A. Michalowicz, in *Logiciels pour la Chimie* (Société Française de Chimie, Paris, 1991), p. 102.
[11]Report on the International Workshops on Standards and Criteria in XAFS, in *X-Ray Absorption Fine Structure: Proceedings of the VI International Conference on X-Ray Absorption Fine Structures*, edited by S. S. Hasnain (Ellis Horwood, New York, 1991), p. 752.
[12]W. Liu and M. Flytzani-Stephanopoulos, J. Catal. **153**, 304 (1995).
[13]G. Balducci, J. Kaspar, P. Fornasiero, M. Graziani, M. S. Islam, and J. D. Gale, J. Phys. Chem. B **101**, 1750 (1997).
[14]L. X. Chen, T. Rajh, Z. Wang, and M. C. Thurnauer, J. Phys. Chem. B **101**, 10688 (1997).
[15]L. X. Chen, T. Raij, W. Jager, J. Nedelijkovic, and M. C. Thurnauer, J. Synchrotron Radiat. **6**, 445 (1999).

[16]F. Farges, J. Non-Cryst. Solids **244**, 25 (1999).
[17]P. Ghigna, G. Spinolo, M. Scavini, A. Tamburini, and A. V. Chadwick, Physica C **253**, 147 (1995).
[18]Y. Okamoto, T. Kubota, H. Gotoh, Y. Ohto, H. Aritani, T. Tanaka, and S. Yoshida, J. Chem. Soc., Faraday Trans. **94**, 3743 (1998).
[19]L. Lu, S. L. Bernasek, and J. Schwartz, Surf. Sci. **458**, 80 (2000).
[20]V. A. Alves, L. A. Silva, S. C. Castro, and F. C. Boodts, J. Chem. Soc., Faraday Trans. **94**, 711 (1998).
[21]A. Y. Stakheev, E. S. Shapiro, and J. Apijok, J. Phys. Chem. **97**, 5668 (1993).
[22]D. R. Mullins, S. H. Overbury, and D. R. Huntley, Surf. Sci. **409**, 307 (1998).